Article

A new 1:1 drug-drug cocrystal of theophylline and aspirin: discovery, characterization and construction of ternary phase diagrams

Shaza Darwish, Jacek Zeglinski, Rama Krishna Gamidi, Rahamatullah Shaikh, Majeda Khraisheh, Gavin M. Walker, and Denise M. Croker

Cryst. Growth Des., **Just Accepted Manuscript** • DOI: 10.1021/acs.cgd.8b01330 • Publication Date (Web): 13 Nov 2018

A new 1:1 drug-drug cocrystal of theophylline and aspirin: discovery, characterization and construction of ternary phase diagrams

Shaza Darwish[1,*], Jacek Zeglinski[1], Gamidi Rama Krishna[1], Rahamatullah Shaikh[1], Majeda Khraisheh[2], Gavin M. Walker[1], Denise M. Croker[1]

[1]Synthesis & Solid State Pharmaceutical Center (SSPC), Bernal Institute, University of Limerick, Limerick, Ireland

[2]Department of Chemical Engineering, College of Engineering, Qatar University, Doha, Qatar

Keywords: Pharmaceutical cocrystal, drug-drug cocrystal, ternary phase diagram, molecular modelling

Abstract

A new 1:1 drug-drug cocrystal of theophylline (THP) and aspirin (ASP) was successfully prepared by liquid assisted grinding, evaporative crystallization and slurry conversion crystallization. The obtained cocrystal was comprehensively characterized by Single Crystal X-ray Diffraction, Powder X-ray diffraction, Differential Scanning Calorimetry, Thermogravimetric analysis, Scanning Electron Microscopy and Fourier Transform Infrared analysis. Ternary phase diagrams (TPDs) were constructed for the obtained cocrystal in isopropyl alcohol at two different temperatures, *i.e*. 20 and 40°C. A narrow stability region was found for the pure THP-ASP cocrystal in the phase diagram at both temperatures. By proper selection of the ratios between THP, ASP and IPA from the stability region, THP-ASP cocrystals could be purely produced by isothermal slurry conversion in IPA. In addition, molecular modelling was deployed to provide mechanistic insights into the formation of this THP-ASP cocrystal system.

Introduction

Cocrystals are defined as crystalline materials comprised of two or more components that are solids under ambient conditions and held together by noncovalent forces.[1-2] Pharmaceutical cocrystals which include at least one active pharmaceutical ingredient (API) in the crystal lattice are becoming an integral part of the pharmaceutical industry. As the components are held together based on intermolecular interactions, cocrystals offer the advantage of improving the physicochemical properties of the APIs without modifying their structural integrity. Hence, the design of new solid forms of APIs, with improved physicochemical properties like stability, melting point, hygroscopicity and solubility by cocrystallization has gained a wide interest.[3-7]

Cocrystal manufacture with a high purity and yield is a challenging task because thermodynamic and kinetic aspects of cocrystal formation remain poorly understood.[8] However, in recent years, construction of ternary phase diagrams (TPDs) has helped to address such issues. TPDs are useful to determine the stability region of a desired cocrystal in a specific solvent and offer the corresponding

stoichiometric ratios of individual components for pure cocrystal formation.[9-13] They are also specifically important for development of crystallization methodologies.[14] Recently, Chiarella et al. have explained the importance of TPDs for the development of preparative procedures for solution crystallization, using 1:1 stochiometric ratio of trans-cinnamic acid and nicotinamide as a model cocrystal.[9] In some cases, the construction of TPDs has led to the discovery of new solid forms of cocrystals for specific systems. For instance, Chadwick et al. found a new solid form of urea–glutaric acid cocrystal when they constructed the TPD in H_2O.[10] Moreover, TPDs assisted the identification of the stability region of a new equimolar cocrystal of p-toluenesulfonamide and triphenylphosphine oxide which was previously known to form one cocrystal of 3:2 ratio.[11]

As an emerging subset of cocrystals, drug-drug cocrystals are made up of two APIs that may not only lead to the modification of the physicochemical properties, but also present new opportunities for the development of synergistic therapies.[15] In addition, drug-drug cocrystals are more patent eligible since they fulfil the criteria of novelty, utility and unpredictability.[16] However, this domain remains underexplored due to the complexity in their design and preparation.[17] Consequently, there is a strong interest and demand to develop cocrystallization methods for drug-drug cocrystals.

Theophylline (THP) is a well-studied component that has been used in the synthesis of various types of cocrystals.[18-20] It is used in the treatment of respiratory diseases, such as asthma therapy.[20] It is the major metabolite of caffeine and can be found in tea, coffee, cocoa beans and chocolate.[21] THP has four anhydrous polymorphs, among which pholymorph II is kinetically stable at room temperature and commercially available. It also has a monohydrated form that occurs frequently due to the hygroscopic nature of THP.[22-29] The structure of THP molecule is shown in Figure 1. It has an imidazole proton, an imidazole nitrogen and two carbonyl groups (one donor and three acceptors) that play significant roles in the formation of hydrogen bonds, which in turns facilitates the synthesis of numerous types of cocrystals with different coformers. It has been proven that the hygroscopic nature of THP was restrained by cocrystallization with different types of acid coformers *via* the formation of O–H(carboxyl)···N(imidazole) and N-H(imidazole)···O=C(carboxyl) hydrogen bonds.[20]

Aspirin (ASP) is considered as GRAS (generally regarded as safe) API that has been employed as a coformer in pharmaceutical cocrystals.[30] It is an acetyl derivative of salicylic acid (Figure 1), which is mainly used in the treatment of pain, inflammation and fever. ASP is known to have three polymorphs, among which polymorph I is the stable phase under ambient condition.[31-34] Moreover, the ASP molecule contains the carboxylic acid functional group which acts as a hydrogen bond acceptor and donor. The ΔpK_a difference between the THP and ASP is -1.8 (pK_a is 1.7 for protonated THP[35] and 3.5 for ASP[36]), hence, THP has the affinity to form a cocrystal with ASP through N–H···O and O–H···O intermolecular interactions.

Accordingly, in this work, we present a new 1:1 THP-ASP cocrystal which can be synthesized by multiple methods. The obtained cocrystal was characterized comprehensively and its structure was successfully solved. Furthermore, molecular modelling was also carried out to understand the mechanism of its formation.

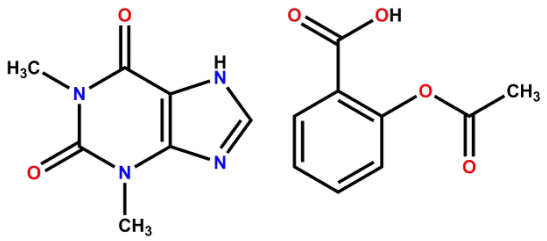

Figure 1. Molecular structures of both theophylline and aspirin molecules.

Experimental Section

Materials and methods

Commercially available THP and ASP (catalogue numbers: J60203.5H and A12488.36 respectively) were purchased from VWR, Alfa Aesar and used as received. The solvent IPA was purchased from VWR, and used without further purification.

Neat and liquid assisted grinding

Equimolar amounts of ASP and THP were ground using a mortar and pestle for 30 min. Liquid assisted grinding (LAG) was performed in a similar way as neat grinding (NG) method except a few drops of IPA were added.

Ball milling (BM)

BM experiments were performed using a Retsch MM400 ball mill. Equimolar amounts of THP and ASP were placed in 25 mL jars containing a 15 mm stainless steel ball per jar. The mill was operated at 25 Hz frequency for 30 min.

Preparation of single crystals

A mixture of THP and ASP (1.5 g, molar ratio 2 : 3) was slurried in 4 mL IPA at 40°C for 24 h. It was then filtered and left for partial evaporation until crystals suitable for single crystal X-ray diffraction (SCXRD) experiments were obtained.

Solubility studies

The solubilities for THP and ASP were measured gravimetrically in IPA at 20 and 40°C respectively. An excess amount of each solid was added to the solvent at the required temperature and agitated in a

Cambridge Reactor Polar Bear Plus instrument. Agitation was then stopped after 24 h and the solid was allowed to settle down for 1 h.

A volume of the sample was filtered using a syringe filter and injected into a preweighed glass vial (W_1) and then weighed (W_2). After allowing the solvent to evaporate, the glass vial was put in an oven at 50°C overnight. The dry weight (W_3) of the vial was recorded after it was allowed to cool down to room temperature (RT). From this final dry mass and the mass of the initial solution, the solubility at the given temperature was calculated using the formula below:

The solubility = $(W_3-W_1)/(W_2-W_3)$ (g of solid/g of solvent) (1)

Construction of the Ternary Phase Diagrams

Slurries of different compositions of THP and ASP in IPA were produced in 30 mL glass vials and agitation was provided by using 10 mm magnetic stirrer bars. The vials were placed in Cambridge Reactor Polar Bear Plus instrument at the specified temperatures (20 and 40°C) for 24 h. Aliquots of solutions were withdrawn after 24 h and the concentrations of THP and ASP were determined by HPLC.

Mass fractions of each substance in the generated IPA solutions were calculated and then plotted on ~~a~~ ternary axis diagrams to generate the appropriate TPDs using ProSim Ternary Diagram software. Eutectic points (Eu) or known as invariant points are fixed solution concentrations at which two solid phases co-exist together in equilibrium. At each temperature, two eutectic points are determined: i) at THP and cocrystal region, Eu_1 and ii) at ASP and cocrystal region, Eu_2. They were determined using the method described by Rodriguez-Hornedo et al,[5] by generating a slurry of the two mentioned solid forms at each point for 24 h.

HPLC Analysis

HPLC was used for the measurement of solubility of THP and ASP in IPA at 20 and 40°C, respectively. The HPLC system was an Agilent 1260 HPLC (Agilent Technologies, Waldbronn, Germany) plus G1311B Quaternary pump, G4212B UV-vis photodiodearray detector, G1322 degasser and Agilent HPLC workstation. The column (Kromasil 250 mm × 4.6 mm, 5 µm) was used for analysis and freshly prepared acetonitrile: acidic H_2O (adjusted pH=3 using ortho-phosphoric acid) (50:50) was set as the mobile phase. The flow rate was 0.75 mL·min^{-1} with simultaneous multichannel UV detection at 260 nm. The injection volume for each sample was 5 µl per sample.

Powder X-ray Diffraction (PXRD)

PXRD patterns were recorded on a PANalytical EMPYREAN diffractometer system using Bragg−Brentano geometry and an incident beam of Cu Kα radiation (λ = 1.5418 Å). Room temperature scans were performed on a spinning silicon sample holder. The diffraction patterns were collected at 40 kV and 40 mA, over a 2θ range from 5-30º, with a scan speed of 0.32857º/s.

Single Crystal X-ray Diffraction (SCXRD)

Suitable single crystals were chosen for SCXRD measurements. The data were collected on a Bruker D8 Quest diffractometer with Mo (λ = 0.71073 Å) sealed tube source at 298 K. The data reduction was performed using Bruker SAINT software. Crystal structures were solved by direct methods using SHELXS and refined by full-matrix least-squares on F^2 with anisotropic displacement parameters for non-H atoms using SHELXL. Hydrogen atoms associated with carbon atoms were fixed in geometrically constrained positions. Hydrogen atoms associated with oxygen and nitrogen atoms were included in the located positions.

Variable temperature PXRD (VT-PXRD)

For VT-PXRD experiments, reflections were collected on Panalytical X'Pert diffractometer (40 kV, 40 mA, Cu Kα1,2, λ = 1.5418 Å) at 10 ºC intervals from 120 to 150°C by heating at 10°C·min^{-1} under N_2 atmosphere. Water cooling system was adopted to control the temperature. Diffraction patterns were collected in the 2θ range of 5-30º. PXRD patterns were also collected at 25°C before and after heating.

Thermogravimetric analysis (TGA)

A Q50 TGA from TA instruments was used for the TGA analysis. Experiments were performed using aluminium pan under a controlled N_2 environment (40 mL·min^{-1}) over a temperature range of 30-550°C with a heating rate 10°C·min^{-1}. The results were further analyzed by using TA instruments Universal 2000 software (Universal V4. 5A).

Differential Scanning Calorimetry (DSC)

Netzch proteus instrument was used to perform the thermal analysis for THP, ASP and THP-ASP samples. Experiments were carried out by using crimped aluminium pan which contains a certain amount of each sample (~5 mg). The experiments were performed over a temperature range of 40 – 280°C at a heating rate of 10°C·min^{-1} under N_2 atmosphere (30 mL·min^{-1}).

Scanning electron microscopy (SEM)

SEM analysis was performed using SU 70 Hitachi instrument. The samples were coated with gold for 2 min at 20 mA.

Fourier Transform Infrared (FTIR) Spectroscopy

FTIR spectra were recorded using Perkin Elmer spectrometer. 12 scans were recorded over a spectral range of 400 - 4000 cm^{-1}.

Molecular Modelling

Density functional theory (DFT) calculations were applied using a Gaussian 09 package[37] to estimate the interaction strength of THP, ASP, and THP-ASP dimers. The equilibrium geometries (gas-phase) are calculated with a B97-D3 Grimme's functional[38] and a Gaussian-type 6-31G(d,p) basis set.[39] The binding energy in each dimer is calculated as follows:

$$\Delta E_{\text{bind}} = E_{\text{AB}} - (E_{\text{A}} + E_{\text{B}}) \quad (2)$$

where E_{AB} is the energy of a dimer AB while E_{A} and E_{B} are energies of the isolated molecules A and B, both being in fully relaxed gas-phase geometries. The energies are calculated using a double hybrid B2PLYP-D3 functional,[40] which combines exact Hartree-Fock exchange with a MP2-like correlation and long-range dispersion corrections; here a basis set of quadruple-ζ valence quality (def2-QZVPP) was used.[41] This methodology has been successfuly applied for small and medium-sized API molecules in recent studies such as salicylic acid,[42] parabens,[43] risperidone,[44] clofazimine,[45] and carbamazepine.[46]

Results and Discussion

PXRD patterns of solids recovered from neat grinding indicated that a new solid phase was formed but significant amounts of starting materials remained (Figure 2a). When a few drops of IPA were added to assist the grinding, the PXRD pattern shows all the main peaks of THP were no longer present and a new solid phase was formed although some peaks were overlapping with those from ASP. This phase can be also prepared by ball milling (BM) assisted with IPA for 30 min. To check if ASP remained in the new phase, DSC experiments were carried out as shown in Figure 2b, which revealed that the onset melting temperature of the new phase is 143°C, which drops between the melting points of the individual components (THP–272°C, and ASP–141°C). There is no endothermal eutectic peak present in the new phase, indicating that the equimolar ASP and THP mixture fully transformed to the new phase. Thus, we assumed that the new phase is a 1:1 ratio of THP-ASP cocrystal.

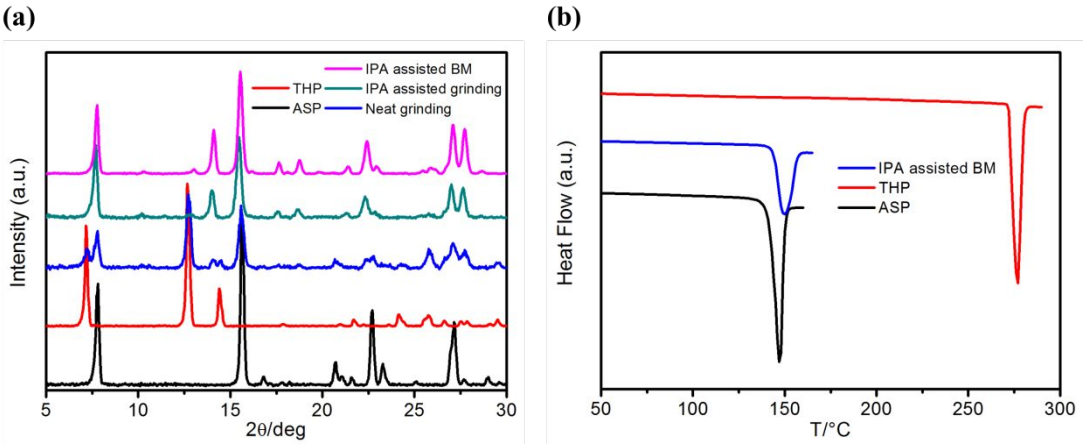

Figure 2. (a) PXRD patterns of ASP, THP and products prepared by neating grinding, IPA assisted grinding and IPA assisted BM, respectively. (b) DSC profiles of ASP, THP and the product prepared by IPA assisted BM.

SCXRD analysis

To verify our assumptions, single crystals were isolated by evaporative crystallization from IPA. SCXRD analysis revealed that the obtained THP–ASP cocrystal crystallizes in the triclinic *P*-1 space group (see Table S1 for full crystallographic information), with one molecule of each component present in the asymmetric unit (Figures 3). The ORTEP diagram of THP-ASP cocrystal is provided in Figure S1. The imidazole hydrogen atom of THP forms a strong N-H···O hydrogen bond with the carboxylic oxygen of ASP while the carboxylic hydrogen atom of ASP froms another strong O-H···O hydrogen bond with the carbonyl oxygen of THP. The two hydrogen bonds lead to a $R_2^2(9)$ ring in the heterodimer. Further, two THP-ASP dimers are connected with each other via moderate C-H (phenyl, ASP)···O (carbonyl, THP) hydrogen bonds, forming a four-molecule cluster (Figure S2). Moreover, the clusters can be repeatedly connected by each other via weak C-H (methyl, ASP)···O (carbonyl, THP) hydrogen bonds, resulting in a 1D tape-like chain (Figure S3). The distances, angles and strengthes of hydrogen bonds are listed in Table S2. As expected, the calculated PXRD pattern from SCXRD data matches well with those experimental PXRD data for IPA assisted grinding and ball milling (Figure 4).

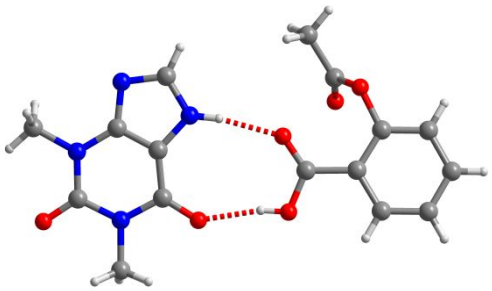

Figure 3. The structure of 1:1 THP-ASP cocrystal, the red dash lines stand for N–H···O and O–H···O hydrogen bonds.

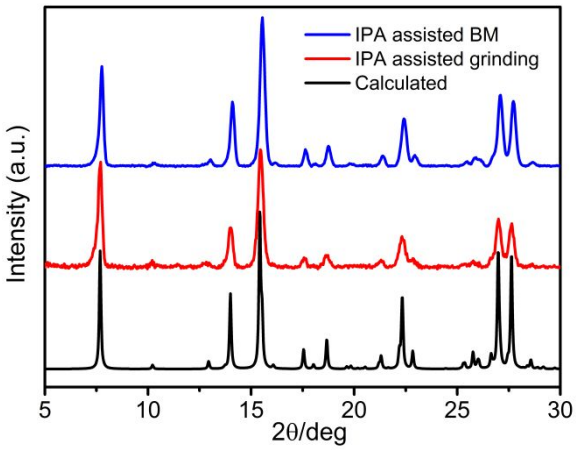

Figure 4. The calculated PXRD pattern of THP-ASP cocrystal (black line) and experimental PXRD pattern for IPA assisted BM product (red line).

Solubility measurements

The solubilities of THP and ASP were determined by gravimetric method in IPA at 20°C and 40°C, respectively, and the values are listed in Table 1. The solubility of ASP is much higher than THP by factors of 43 and 48 times at 20°C and 40°C, respectively.

Table 1. Measured solubility values of THP and ASP in IPA**.**

Temperature (°C)	THP concentration (mg/mL)	THP concentration (M)	ASP concentration (mg/mL)	ASP concentration (M)
20	2.27±0.14	0.0126	96.1±2.7	0.5339
40	5.60±0.01	0.0326	241±4	1.3389

The two invariant (eutectic) points were determined experimentally and listed in Table 2 and Table 3 at 20 and 40°C respectively.

Table 2. Invariant points at 20°C.

	Solid forms in equilibrium	Mass fraction of THP	Mass fraction of ASP	Mass fraction of IPA	THP concentration (M)	ASP concentration (M)
Point 1	THP and THP-ASP cocrystal	0.0037	0.0467	0.9495	0.0170	0.2146
Point 2	ASP and THP-ASP cocrystal	0.0018	0.0939	0.9043	0.0086	0.4530

Table 3. Invariant points at 40°C.

	Solid forms in equilibrium	Mass fraction of THP	Mass fraction of ASP	Mass fraction of IPA	THP concentration (M)	ASP concentration (M)
Point 1	THP and THP-ASP cocrystal	0.0079	0.1235	0.8685	0.0399	0.6206
Point 2	ASP and THP-ASP cocrystal	0.0050	0.2006	0.7944	0.0274	1.1015

Construction and interpretation of ternary phase diagrams

In order to gain some insights into the thermodynamics of the THP-ASP cocrystal system, TPDs were constructed at 20 and 40°C in IPA respectively (Figure 5 and Figure 6). For clarity, the diagrams were plotted using mass fractions. Both diagrams show unsymmetrical behaviour, a trend that is common when there is a wide difference in solubility between the pure drug and coformer.[9]

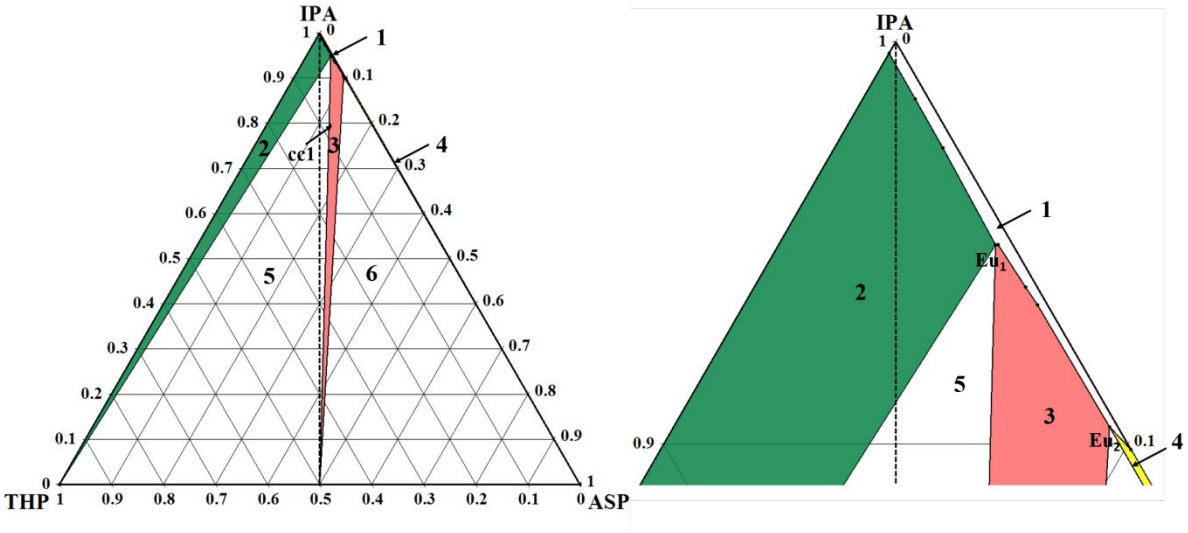

Figure 5. Ternary phase diagram (Left) and the expansion of the top diagram (Right) for the THP−ASP−IPA system at 20°C.

The TPD at 20°C (Figure 5) is divided into six regions. Region 1 represents an undersaturated solution. Regions 2, 3 and 4 signify a solution in equilibrium with the solid phases of THP, THP-ASP cocrystal and ASP respectively. As for regions 5 and 6, they represent the coexistence of cocrystal with THP and ASP respectively.

The region of cocrystal stability (region 3) is skewed toward the ASP axis as its solubility is much higher than the solubility of THP. The 1:1 component stoichiometric line does not intersect the solubility curve for the 1:1 cocrystal, resulting an incongruent phase diagram. This implies that for an equimolar mixture of THP and ASP, one cannot get a suspension of pure THP-ASP cocrystals no matter how much IPA is used. Because the cocrystal phase on its own will transform either to the mixture of cocrystal and THP (zone 5) or to THP (Zone 2) according to the amount of solvent used. As a result, the solubility of the cocrystal cannot be readily determined as it transforms to the most stable drug form in solution.[5]

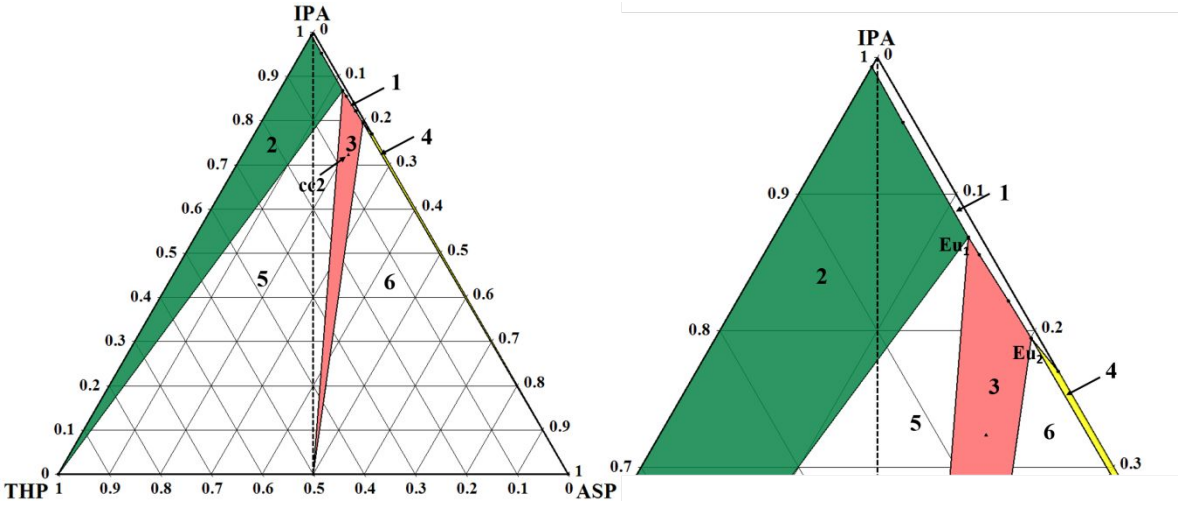

Figure 6. Ternary phase diagram (Left) and the expansion of the top diagram (Right) for the THP−ASP−IPA system at 40°C.

The same regions are present at 40°C (Figure 6). However, at higher temperature, the solubility of both THP and ASP increased and the diagram was pushed downward ,making the liquidus region more significant and clear. It is found that temperature has significant effects on the size and position of the thermodynamic stability regions. For instance, the cocrystal region became more skewed toward the ASP axis, the distance between the solvent apex and the cocrystal solubility curve became longer and the undersaturated region occupied a larger area. Obviously, increasing temperature has increased the solubilities of both drugs by different amounts which resulted in an increase in the difference between the solubilities and therefore making the diagram even more asymmetric. Although the cocrystal still dissolved incongruently, pure single crystals can be prepared by choosing the appropriate point from the diagram.

Isothermal slurry cocrystallisation

To check the reliability of TPDs, two combination points 'cc1' and 'cc2' from region 3 at each temperature were selected to prepare THP–ASP cocrystal by isothermal slurry conversion crystallization method in IPA. The PXRD patterns of cocrystals obtained from this method match well with the calculated PXRD pattern (Figure 7a). DSC analysis (Figure 7b) also reveals the purity of THP-ASP cocrystal. TGA profiles show that the decomposition of the cocrystal starts around 145°C, comparable with that of ASP but with different mass loss rate. VT-PXRD data is also consistent with TGA, where the cocrystal dissociates at 150°C, suggesting the formation of THP crystals after the ASP decomposition (Figure 8). The FTIR spectrum of the THP-ASP cocrystal is, to a large extent, a superposition of the ASP and THP spectra. The major difference is the presence of a high-intensity band at 1631 cm^{-1}, which in ASP and THP appears as a low-intensity shoulder (Figure S4). SEM analysis was carried out to visualise and compare the external appearance of ASP, THP and the newly formed cocrystal (Figure S5). It shows that ASP presents flat block crystal habit and THP presents as elongated needle shape. However, the new THP-ASP cocrystal could be differentiated by its distinct polyhydral shape.

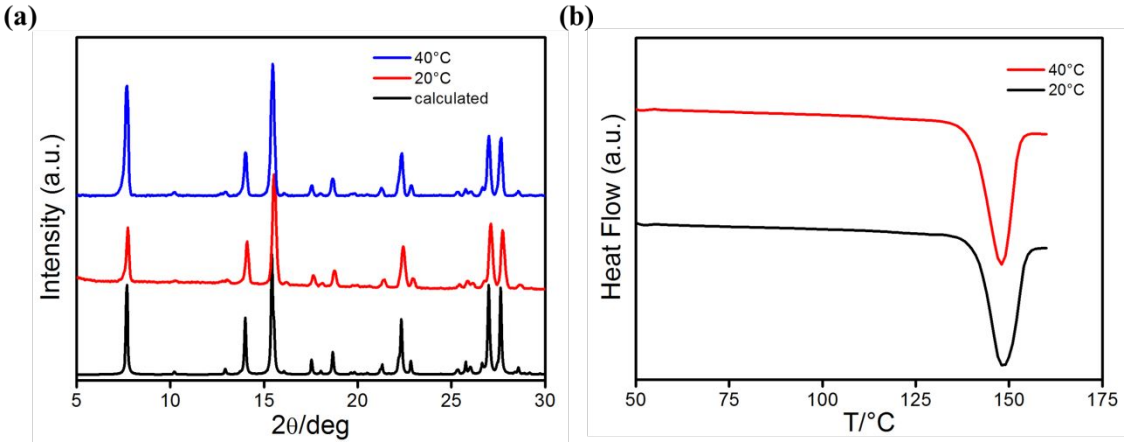

Figure 7. (a) PXRD patterns and (b) DSC curves of the obtained cocrystal using isothermal slurry conversion crystallization method at 20 and 40°C

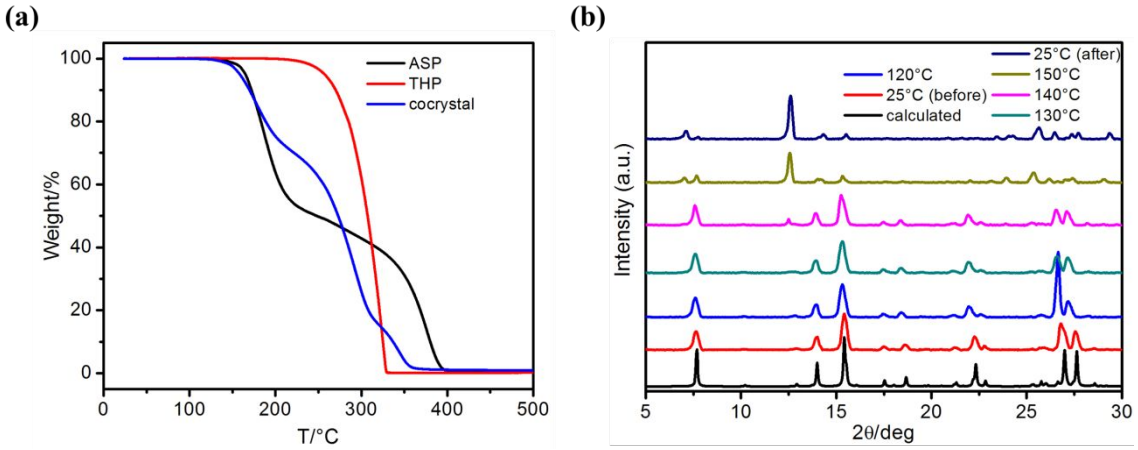

Figure 8. (a) TGA analysis of THP, ASP and THP–ASP cocrystal; (b) VT-PXRD of the prepared THP-ASP cocrystal.

Mechanistic insight

In effort to gain a molecular-level understanding of the formation of THP–ASP cocrystal, we calculated the binding energies in dimers of THP, ASP and the resultant THP-ASP cocrystal by density function theory (Figure 9). Our computations show that THP dimer (F II) comprises a strong N–H···N and a weak C=O···H–C hydrogen bonding (ΔE_{bind} = -46.9 kJ/mol). ASP dimer (F I) forms a centrosymmetric H-bonded dimer due to interactions of its carboxyl groups; this results in creation of two strong C=O···H–O H-bonds and yields ΔE_{bind} = -66.9 kJ/mol. The THP–ASP dimer is stabilised by binding energy of -71.2 kJ/mol, which results from interactions of two strong H-bonds: C=O_{THP}···H–O and C=O_{ASP}···H–N. Thus, the order of bonding energy is THP dimer (F II) < ASP dimer (F I) < THP–ASP dimer, rationalising the formation potential of THP-ASP solid.

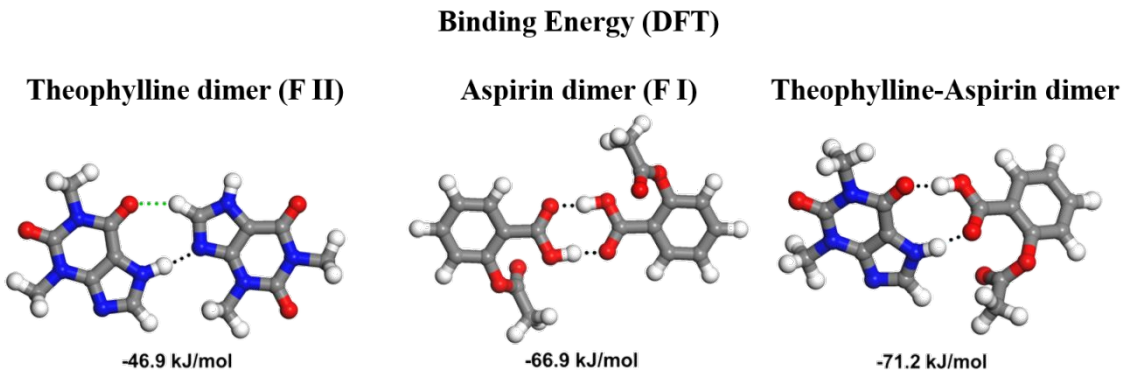

Figure 9. DFT binding energy calculated for dimers of THP (F II), ASP (F I), and THP-ASP cocrystal.

Conclusion

A new 1:1 drug-drug cocrystal of THP-ASP was synthesised and characterized. The construction of TPDs clearly identified the stability regions for pure THP-ASP cocrystal formation in IPA at 20 and 40°C, allowing the rationalization of the experimental conditions for future manufacture. The TPDs indicated that THP-ASP cocrystal was stable in a narrow region in IPA. The melting point of THP-ASP cocrystal is much closer to that of ASP rather than THP. The new cocrystal displayed different crystal habit to the starting materials. The mechanistic insight behind the cocrystal formation was also studied and the preferential formation of THP-ASP cocrystals was proved by DFT binding energy calculations.

Supporting Information

X-ray crystallographic information, supplementary figures of crystal structures, FTIR and SEM images are available in SI. The cif file for the THP-ASP cocrystal have been deposited with the Cambridge Crystallographic Data Centre, CCDC number 1821703.

Acknowledgements

This work was funded by Science Foundation Ireland (SFI) under the following grant: Model Predictive Control of Continuous Pharmaceutical Processes - (13/IA/1980). J. Zeglinski acknowledges the Science Foundation Ireland (SFI) and Higher Education Authority funded Irish Centre for High End Computing (ICHEC) for access to computational facilities.

References

1. Desiraju, G. R., Crystal and co-crystal. *CrystEngComm* **2003,** *5* (82), 466-467.
2. Bond, A. D., What is a co-crystal? *CrystEngComm* **2007,** *9* (9), 833-834.
3. Almarsson, O.; Zaworotko, M. J., Crystal engineering of the composition of pharmaceutical phases. Do pharmaceutical co-crystals represent a new path to improved medicines? *Chem. Commun.* **2004,** (17), 1889-1896.
4. Childs, S. L.; Stahly, G. P.; Park, A., The Salt−Cocrystal Continuum: The Influence of Crystal Structure on Ionization State. *Mol. Pharm.* **2007,** *4* (3), 323-338.

5. Good, D. J.; Rodríguez-Hornedo, N., Solubility Advantage of Pharmaceutical Cocrystals. *Cryst. Growth Des.* **2009,** *9* (5), 2252-2264.
6. Schultheiss, N.; Newman, A., Pharmaceutical Cocrystals and Their Physicochemical Properties. *Cryst. Growth Des.* **2009,** *9* (6), 2950-2967.
7. Shan, N.; Zaworotko, M. J., The role of cocrystals in pharmaceutical science. *Drug Discovery Today* **2008,** *13* (9–10), 440-446.
8. Gagnière, E.; Mangin, D.; Puel, F.; Rivoire, A.; Monnier, O.; Garcia, E.; Klein, J.-P., Formation of co-crystals: kinetic and thermodynamic aspects. *J. Cryst. Growth* **2009,** *311* (9), 2689-2695.
9. Chiarella, R. A.; Davey, R. J.; Peterson, M. L., Making Co-Crystals The Utility of Ternary Phase Diagrams. *Cryst. Growth Des.* **2007,** *7* (7), 1223-1226.
10. Chadwick, K.; Davey, R.; Sadiq, G.; Cross, W.; Pritchard, R., The utility of a ternary phase diagram in the discovery of new co-crystal forms. *CrystEngComm* **2009,** *11* (3), 412-414.
11. Croker, D. M.; Foreman, M. E.; Hogan, B. N.; Maguire, N. M.; Elcoate, C. J.; Hodnett, B. K.; Maguire, A. R.; Rasmuson, Å. C.; Lawrence, S. E., Understanding the p-Toluenesulfonamide/Triphenylphosphine Oxide Crystal Chemistry: A New 1:1 Cocrystal and Ternary Phase Diagram. *Cryst. Growth Des.* **2012,** *12* (2), 869-875.
12. Hong, C.; Xie, Y.; Yao, Y.; Li, G.; Yuan, X.; Shen, H., A Novel Strategy for Pharmaceutical Cocrystal Generation Without Knowledge of Stoichiometric Ratio: Myricetin Cocrystals and a Ternary Phase Diagram. *Pharm. Res.* **2015,** *32* (1), 47-60.
13. Jayasankar, A.; Reddy, L. S.; Bethune, S. J.; Rodríguez-Hornedo, N., Role of Cocrystal and Solution Chemistry on the Formation and Stability of Cocrystals with Different Stoichiometry. *Cryst. Growth Des.* **2009,** *9* (2), 889-897.
14. Kudo, S.; Takiyama, H., Production method of carbamazepine/saccharin cocrystal particles by using two solution mixing based on the ternary phase diagram. *J. Cryst. Growth* **2014,** *392*, 87-91.
15. Aitipamula, S.; Chow, P. S.; Tan, R. B. H., Trimorphs of a pharmaceutical cocrystal involving two active pharmaceutical ingredients: potential relevance to combination drugs. *CrystEngComm* **2009,** *11* (9), 1823-1827.
16. Sekhon, B. S., Drug-drug co-crystals. *DARU J. Pharm. Sci.* **2012,** *20* (1), 45-45.
17. Bordignon, S.; Cerreia Vioglio, P.; Priola, E.; Voinovich, D.; Gobetto, R.; Nishiyama, Y.; Chierotti, M. R., Engineering Codrug Solid Forms: Mechanochemical Synthesis of an Indomethacin–Caffeine System. *Cryst. Growth Des.* **2017,** *17* (11), 5744-5752.
18. Yeh, K. L.; Lee, T., Intensified Crystallization Processes for 1: 1 Drug–Drug Cocrystals of Sulfathiazole–Theophylline, and Sulfathiazole–Sulfanilamide. *Cryst. Growth Des.* **2018,** *18* (3), 1339-1349.
19. Rossi, F.; Cerreia Vioglio, P.; Bordignon, S.; Giorgio, V.; Nervi, C.; Priola, E.; Gobetto, R.; Yazawa, K.; Chierotti, M. R., Unraveling the Hydrogen Bond Network in a Theophylline-Pyridoxine Salt Cocrystal by a Combined X-ray Diffraction, Solid-State NMR, and Computational Approach. *Cryst. Growth Des.* **2018**, *18* (4), 2225-2233.
20. Trask, A. V.; Motherwell, W. D. S.; Jones, W., Physical stability enhancement of theophylline via cocrystallization. *Int. J. Pharm.* **2006,** *320* (1-2), 114-123.
21. Jafari, M. T.; Rezaei, B.; Javaheri, M., A new method based on electrospray ionisation ion mobility spectrometry (ESI-IMS) for simultaneous determination of caffeine and theophylline. *Food Chem.* **2011,** *126* (4), 1964-1970.
22. Ebisuzaki, Y.; Boyle, P. D.; Smith, J. A., Methylxanthines. I. Anhydrous Theophylline. *Acta Crystallogr. Sect. C* **1997,** *53* (6), 777-779.
23. Fucke, K.; McIntyre, G. J.; Wilkinson, C.; Henry, M.; Howard, J. A. K.; Steed, J. W., New Insights into an Old Molecule: Interaction Energies of Theophylline Crystal Forms. *Cryst. Growth Des.* **2012,** *12* (3), 1395-1401.
24. Khamar, D.; Bradshaw, I. J.; Hutcheon, G. A.; Seton, L., Solid State Transformations Mediated by a Kinetically Stable Form. *Cryst. Growth Des.* **2012,** *12* (1), 109-118.

25. Khamar, D.; Pritchard, R. G.; Bradshaw, I. J.; Hutcheon, G. A.; Seton, L., Polymorphs of anhydrous theophylline: stable form IV consists of dimer pairs and metastable form I consists of hydrogen-bonded chains. *Acta Crystallogra. Sect. C* **2011,** *67* (12), o496-o499.
26. Pinon, A. C.; Rossini, A. J.; Widdifield, C. M.; Gajan, D.; Emsley, L., Polymorphs of Theophylline Characterized by DNP Enhanced Solid-State NMR. *Mol. Pharm.* **2015,** *12* (11), 4146-4153.
27. Seton, L.; Khamar, D.; Bradshaw, I. J.; Hutcheon, G. A., Solid State Forms of Theophylline: Presenting a New Anhydrous Polymorph. *Cryst. Growth Des.* **2010,** *10* (9), 3879-3886.
28. Sun, C.; Zhou, D.; Grant, D. J. W.; Young, V. G., Jr, Theophylline monohydrate. *Acta Crystallogra. Sect. E: Structure Reports Online* **2002,** *58* (4), o368-o370.
29. Zhang, S.; Fischer, A., A monoclinic polymorph of theophylline. *Acta Crystallogra. Sect. E: Struct. Rep. Online* **2011,** *67* (Pt 12), o3357-o3357.
30. Cheney, M. L.; Weyna, D. R.; Shan, N.; Hanna, M.; Wojtas, L.; Zaworotko, M. J., Coformer selection in pharmaceutical cocrystal development: a case study of a meloxicam aspirin cocrystal that exhibits enhanced solubility and pharmacokinetics. *J. Pharm. Sci.* **2011,** *100* (6), 2172-2181.
31. Bond, A. D.; Boese, R.; Desiraju, G. R., On the Polymorphism of Aspirin: Crystalline Aspirin as Intergrowths of Two "Polymorphic" Domains. *Angew. Chem. Int. Ed.* **2007,** *46* (4), 618-622.
32. Chan, E. J.; Welberry, T. R.; Heerdegen, A. P.; Goossens, D. J., Diffuse scattering study of aspirin forms (I) and (II). *Acta Crystallogra. Sect. B: Struct. Sci.* **2010,** *66* (Pt 6), 696-707.
33. Vishweshwar, P.; McMahon, J. A.; Oliveira, M.; Peterson, M. L.; Zaworotko, M. J., The Predictably Elusive Form II of Aspirin. *J. Am. Chem. Soc.* **2005,** *127* (48), 16802-16803.
34. Shtukenberg, A. G.; Hu, C. T.; Zhu, Q.; Schmidt, M. U.; Xu, W.; Tan, M.; Kahr, B., The Third Ambient Aspirin Polymorph. *Cryst. Growth Des.* **2017,** *17* (6), 3562-3566.
35. Childs, S. L.; Stahly, G. P.; Park, A., The salt−cocrystal continuum: the influence of crystal structure on ionization state. *Mol. Pharmaceut.* **2007,** *4* (3), 323-338.
36. Florey, K., Aspirin. In *Analytical Profiles of Drug Substances*, Florey, K., Ed. Academic Press: 1979; Vol. 8, pp 1-46.
37. Frisch, M.; Trucks, G.; Schlegel, H.; Scuseria, G.; Robb, M.; Cheeseman, J.; Scalmani, G.; Barone, V.; Mennucci, B.; Petersson, G., 09 Gaussian D. 01 Revision. **2013**.
38. Grimme, S.; Ehrlich, S.; Goerigk, L., Effect of the damping function in dispersion corrected density functional theory. *J. comput. chem.* **2011,** *32* (7), 1456-1465.
39. Rassolov, V. A.; Ratner, M. A.; Pople, J. A.; Redfern, P. C.; Curtiss, L. A., 6-31G* basis set for third-row atoms. *J. Comput. Chem.* **2001,** *22* (9), 976-984.
40. Schwabe, T.; Grimme, S., Double-hybrid density functionals with long-range dispersion corrections: higher accuracy and extended applicability. *Phys. Chem. Chem. Phys.* **2007,** *9* (26), 3397-3406.
41. Weigend, F.; Ahlrichs, R., Balanced basis sets of split valence, triple zeta valence and quadruple zeta valence quality for H to Rn: Design and assessment of accuracy. *Phys. Chem. Chem. Phys.* **2005,** *7* (18), 3297-3305.
42. Khamar, D.; Zeglinski, J.; Mealey, D.; Rasmuson, Å. C., Investigating the Role of Solvent–Solute Interaction in Crystal Nucleation of Salicylic Acid from Organic Solvents. *J. Am. Chem. Soc.* **2014,** *136* (33), 11664-11673.
43. Zhang, S.; Rasmuson, Å. C., Thermodynamics and Crystallization of the Theophylline–Glutaric Acid Cocrystal. *Cryst. Growth Des.* **2013,** *13* (3), 1153-1161.
44. Mealey, D.; Zeglinski, J.; Khamar, D.; Rasmuson, Å. C., Influence of solvent on crystal nucleation of risperidone. *Faraday discuss.* **2015,** *179*, 309-328.
45. Bannigan, P.; Zeglinski, J.; Lusi, M.; O'Brien, J.; Hudson, S. P., Investigation into the Solid and Solution Properties of Known and Novel Polymorphs of the Antimicrobial Molecule Clofazimine. *Cryst. Growth Des.* **2016,** *16* (12), 7240-7250.
46. Padrela, L.; Zeglinski, J.; Ryan, K. M., Insight into the Role of Additives in Controlling Polymorphic Outcome: A CO2-Antisolvent Crystallization Process of Carbamazepine. *Cryst. Growth Des.* **2017,** *17* (9), 4544-4553.

For table of contents use only

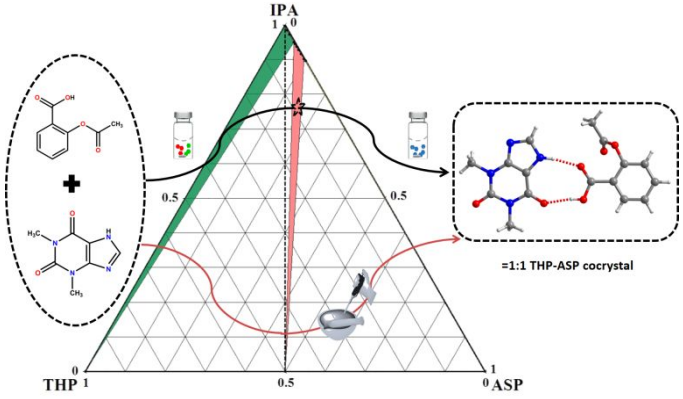

A new 1:1 drug-drug cocrystal of theophylline and aspirin: discovery, characterization and construction of ternary phase diagrams

Shaza Darwish[1,*], Jacek Zeglinski[1], Gamidi Rama Krishna[1], Rahamatullah Shaikh[1], Majeda Khraisheh[2], Gavin M. Walker[1], Denise M. Croker[1]

[1]Synthesis & Solid State Pharmaceutical Center (SSPC), Bernal Institute, University of Limerick, Limerick, Ireland

[2]Department of Chemical Engineering, College of Engineering, Qatar University, Doha, Qatar